Lawrence Berkeley National Laboratory
Lawrence Berkeley National Laboratory

Title
Actinic defect counting statistics over 1 cm2 area of EUVL mask blank

Permalink
https://escholarship.org/uc/item/6zp799ts

Authors
Jeong, Seongtae
Lai, Chih-Wei
Rekawa, Seno
et al.

Publication Date
2000-02-18

eScholarship.org Powered by the California Digital Library
University of California

Actinic defect counting statistics over 1 cm^2 area of EUVL mask blank

Seongtae Jeong[1], Chih-Wei Lai[1,2], Seno Rekawa[1], Chris C Walton[3], Jeffrey Bokor[1,4]

[1] Center for X-Ray Optics, Lawrence Berkeley National Laboratory, Berkeley, CA 94720
[2] Graduate Group of Applied Science and Technology, University of California, Berkeley, CA 94720
[3] Lawrence Livermore National Laboratory, Livermore, CA 94550
[4] Department of Electrical Engineering and Computer Science, University of California, Berkeley, CA 94720

ABSTRACT

As a continuation of comparison experiments between EUV inspection and visible inspection of defects on EUVL mask blanks, we report on the result of an experiment where the EUV defect inspection tool is used to perform at-wavelength defect counting over 1 cm^2 of EUVL mask blank. Initial EUV inspection found five defects over the scanned area and the subsequent optical scattering inspection was able to detect all of the five defects. Therefore, if there are any defects that are only detectable by EUV inspection, the density is lower than the order of unity per cm^2. An upgrade path to substantially increase the overall throughput of the EUV inspection system is also identified in the manuscript.

Keywords: mask, defect, inspection, roughness, phase defect

1. INTRODUCTION

Extreme ultraviolet lithography(EUVL) proposes to use 11-15 nm EUV radiation and multilayer coated reflective optics to print integrated circuit patterns with less than 100 nm feature size. The mask architecture proposed for EUVL is also a reflective mask composed of circuit patterns formed with EUV absorbers on top of the multilayer reflective coating on a robust substrate. Because a defect on the mask can have an adverse effect on the final printing, there has been an active research effort on defect reduction/inspection and characterization on EUVL mask. A defect can occur either in the absorber pattern or on top of the multilayer as particles. These types of defect can either be repaired or be subject to cleaning procedures. However, a defect underneath the multilayer is very hard to repair or remove. Furthermore, a defect underneath the multilayer with subsequent conformal multilayer growth gives rise to a phase shift in the reflected wavefront. Because EUVL uses radiation around 13 nm, a substrate defect with height as small as 3 nm might impart substantial phase shift.

There are intensive research and development efforts to reduce the number of defects added during multilayer deposition or defects preexisting on the substrate, and the metrology for defect inspection is an integral part of these efforts. Currently, commercial wafer defect inspection tools such as SP1 from KLA-Tencor and Constellation from ADE are used to inspect EUV mask blanks. These tools possess a high throughput and a very high defect sensitivity. However, because the optical properties of multilayer coatings at visible wavelength (at which the wafer defect inspection tool operates) are qualitatively different from those at the EUV wavelength, it must be determined whether such wafer defect inspection tools can capture all the printable defects on EUVL mask blanks. In particular, defects with a height of several nanometers display a very small scattering cross section at visible wavelength as compared to their lateral physical sizes, as well as the EUV scattering cross section[1,2]. The current strategy adopted by the Extreme Ultraviolet Limited Liability Company (EUV LLC) program is to seek correlations between the response of defects to non-EUV inspection tools and their EUV responses so that more economic non-EUV inspection tools can be used for the ultimate commercial production environment. In order to study the at-wavelength properties of defects found on EUVL mask blanks, a prototype EUV inspection system has

been built and used for various experiments comparing the visible responses of defects and their EUV responses. The EUV inspection system is based on raster scanning the EUVL mask blank under a focused EUV beam while monitoring both increase in scattering and decrease in specular reflectivity due to defects[3].

The comparison experiments performed include programmed defect experiments and cross correlation experiments. In the programmed defect experiment, defects of known size and known properties were deliberately fabricated with lithographic techniques. A sample with programmed defects was inspected both by visible inspection tools and the EUV inspection tool and the inspection results were compared[4]. In the "cross correlation experiment", native defects on an EUVL mask blank are first found, mapped and sized by a visible inspection tool. Later the same sample is then loaded in the EUV inspection tool and a small area around each defect is scanned to probe their EUV response [2]. Most of the defects found by the visible inspection tool were detected by the EUV inspection tool, including defects with sub-100 nm dimension. The cross correlation experiments showed a general correlation between EUV inspection results and visible inspection results on the given set of real defects. Those experiments also indicated that EUV inspection is very sensitive to low aspect ratio substrate defects compared to the visible light scattering inspection while visible inspection tool might be more sensitive for another type of defects such as particles on top of the multilayer. Another question crucial to establishing the correlation between the visible inspection tool and the EUV inspection tool is whether defects found by the EUV inspection tool can be found by visible inspection tools. This experiment, complimentary to the cross correlation experiment, involves scanning an area of EUVL mask blank looking for defects in the current EUV inspection system. This type of experiment is referred to as "at-wavelength defect counting experiment" and is the subject of this paper.

We report on the result of an experiment where the EUV inspection tool is used to perform at-wavelength defect counting over 1 cm^2 of EUVL mask blank. The scan area that can be covered is limited due to the low throughput of the current EUV inspection tool. The defect detection sensitivity and limitations of the current EUV inspection tool in terms of its scanning speed and cleanliness of sample handling are described in section II. The experimental procedure and the results are described in section III. In section IV, a technical pathway is discussed to achieve a scanning speed fast enough to scan a full mask blank within a day.

II. REVIEW OF THE CURRENT INSPECTION SYSTEM

II.1 Scanning speed of the current EUV inspection system

Through previous programmed defect experiments and cross correlation experiments, the current EUV inspection tool has been shown to detect sub-100 nm defects, comparable to that of its visible counterpart[2,4]. Especially, the dark field detection channel has shown a very high sensitivity to defects of small size, compared to the corresponding bright field. The defect sensitivity is related to the signal-to-noise ratio, i.e. the signal level achieved for the given defect size versus the noise level at a given dwell time. The signal level for a given defect size is expected to scale as the ratio of the defect footprint to the beam area[2]. For example, based on a pure absorption of EUV radiation[5], a defect with 100 nm lateral size is expected to generate 0.1 % change in the specularly reflected beam intensity (bright field) when the beam area is 10 μm^2. When the spot size is reduced to 1 μm^2, the expected signal level for 100 nm defect is 1 %. The dark field signal level is more complicated to estimate as was shown in reference [2] where there is a significant data spread when the dark field signal is plotted against the bright field signal for various kinds of defects. The actual signal level is expected to vary depending on the nature of the defect (whether it gives rise to phase effect or amplitude effect), height of the defect and its roughness. Even more complicating is the fact that there is an appreciable scattering (on the order of 0.1% of incident photons are scattered into the dark field detector of 0.035sr solid angle) into the dark field detector due to the roughness in the multilayer which might vary from sample to sample depending on the substrate roughness, growth condition and history of sample processing. This diffuse background scattering act as a background signal in the dark field channel. The spatial variation of this dark field background scattering will limit the defect detection sensitivity in the dark field[4]. However, even a conservative estimate from the experimental data from cross correlation experiments shows that a 100 nm defect will generate at least 6% change in the amount of photons collected in the dark field compared to the clear (no-defect) region.

Therefore, to detect 100 nm defects, the system needs to be able to capture 0.1% change in the bright field or 6% change in the dark field with adequate signal to noise ratio.

There are several noise sources contributing to the fluctuation of the signal detected in the bright field and/or dark field. The dependence of the fluctuation level on the dwell time per pixel, i.e. integration time is an important consideration in determining the shortest possible dwell time per pixel without compromising the detection sensitivity. The dominant noise sources to be considered in this section are shot noise, vibration induced noise and spatial variation of the dark field background signal level due to the substrate roughness. Other noise sources such as electrical noise are not the significant noise source at least in the current experimental environment. The shot noise is a fundamental noise due to the discrete particle nature of the incident photons. The *relative* variation inversely scales with the square root of the number of photons detected. The shot noise level in the bright field and dark field can be estimated as follows. If we denote the photon flux incident upon the sample as N_0 photons per second, the dwell time per pixel as T, the multilayer reflectivity as R and assume that the detection efficiency of the bright field detector (photodiode) is close to unity, the number of photons detected by the bright field detector is N_0TR. Then the shot noise level is $1/\sqrt{N_0TR}$. The dark field signal is composed of a diffuse background scattering on the order of 0.5 % of the bright field photon flux. The detection efficiency of the dark field detector (a microchannel plate) at this EUV wavelength is estimated to be 7%. Therefore, the number of photons collected in the dark field detector is (0.005)(0.07) N_0TR and the shot noise level is $1/\sqrt{(0.005)(0.07)N_0TR}$. In both cases, the shot noise level in the bright field scales with the inverse square root of the dwell time at given incident photon flux.

While the shot noise arises from a fundamental particle nature of the incident beam, the vibration of the optical elements in the system contributes to the overall noise level through fluctuation in the total beam energy transmitted through various apertures in the inspection system and beamline. The most obvious aperture is the pinhole that is placed in the object plane of the Kirkpatrick-Baez focusing optics to achieve a small spot size. Also, the beam from the synchrotron radiation source can overfill the beamline mirrors acting effectively as apertures. When the relative position between the aperture and the beam with non-uniform profile changes, the transmitted intensity through the aperture changes accordingly. The vibration-induced noise is rather difficult to estimate because it is dependent on a specific environment in which the EUV inspection system operates. The most straightforward way to estimate the vibration-induced noise is through actual measurement. When the bright field signal is observed over time with pixel dwell time of 10 ms, the standard deviation of the fluctuation is 0.35% of the dc signal level which is much higher than the estimated shot noise contribution. Figure 1 compares the power spectrum of the bright field signal (thick line) with the vibration spectrum of the horizontal deflection mirror (M1 mirror) tank in the horizontal direction (thin line)[6], measured by an accelerometer. The noise spectrum displays several dominant peaks that also appear in the mirror tank vibration spectrum. Because the fluctuation level of the bright field

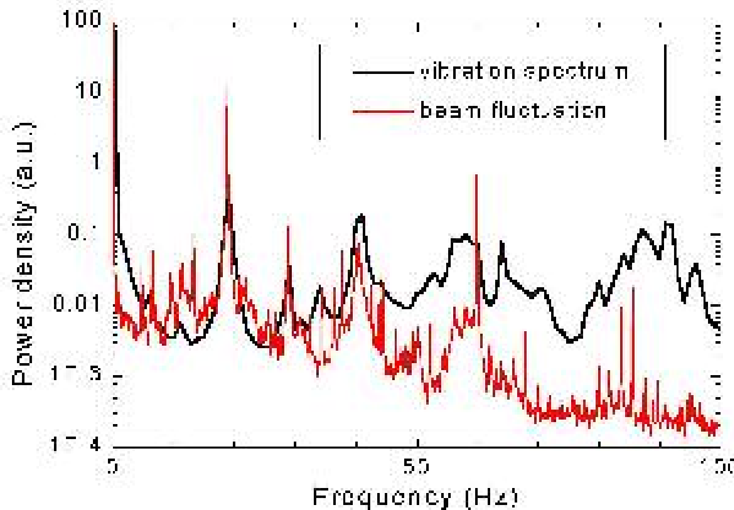

Figure 1. The acceleration spectrum (Thick Line) of the M1 tank in the horizontal direction along with the fluctuation spectrum of the photodiode (Thin Line). The vertical scale is logarithmic. Several dominant peaks coincide between two spectra.

signal is dominated by these peaks (note that the vertical scale is logarithmic), it is concluded that the horizontal vibration of the M1 is the dominant noise source in the bright field signal. The reason why the M1 mirror vibration is so pronounced in the fluctuation in the bright field signal is that the distance between M1 and the pinhole is 11.8 m. Therefore, angular movement of magnitude of 1 μrad can produce a 11.8 μm horizontal displacement of the beam whose size is 300 μm full width at half maximum. Furthermore, M1 is the first mirror that accepts the broadband synchrotron source and it is cooled with circulating water to relieve the heat load. The water flow is suspected to add to the high frequency vibration. Careful study of vibration spectrum of other mirror tanks reveal that the vertical deflection mirror (M3) in the beamline[6] also generates angular deflection of the beam but the distance between the mirror and pinhole is 3 m, which is almost one fourth of that between M1 and the pinhole. Therefore, the effect of vibration of M3 is not as severe as that of M1 in normal operating conditions. It is important to note that the level of bright field fluctuation induced by the vibration of optical elements in the beamline crucially depends on the alignment of the beam center with respect to the center of the pinhole. For example, when the pinhole is positioned intentionally off the center of the beam, it is clearly observed that the *relative* fluctuation level (standard deviation divided by the mean of the bright field signal) increases rapidly to a level as high as 5 % due to the increased beam intensity slope. This effect is more pronounced in the vertical position of the beam relative to the pinhole due to a small spot size (100 μm) in the vertical direction, i.e. increased slope of the beam. Therefore, it is important to achieve the "optimum" overlap of the beam profile and the pinhole in both horizontal and vertical directions to minimize the fluctuation level in the bright field. Unfortunately, it is frequently observed that over the period of four to six hours, the beam position slowly drifts in the horizontal direction and, less frequently, also in the vertical direction. This slow drift in the beam position increases the magnitude of vibration-induced noise and beamline realignment at several hours' interval is necessary to achieve reasonable noise level. The vibration-induced noise level decreases as the dwell time increases due to the bandwidth narrowing of the detection system. The exact functional dependence of the vibration-induced noise level on the integration time or dwell time depends on the noise spectral content. It is reasonable to expect that the noise spectral content is concentrated in the low frequency region (below a few hundred hertz) due to the nature of the mechanical vibration. If this is the case, the vibration induced noise will level off below a certain time constant. Currently, efforts are underway to reduce the noise with active feedback, signal processing and noise source minimization. Further discussion is found in section IV. The vibration-induced noise affects the dark field signal exactly the same way as it does in the bright field signal. However, in the dark field signal, the vibration is not a dominant noise source because the noise in the dark field is generally dominated by either shot-noise or background fluctuations as shown below.

Another important noise source is dark field background signal fluctuation, as was mentioned earlier in the section. This is a unique noise source for the dark field detection. The *position*-dependent dark field fluctuation introduces noise just as other *temporal* noise source does. However, because it is dependent on the position, the fluctuation level does not depend on the dwell time per pixel. The relative level of dark field background fluctuation is 0.8% for most unpatterned multilayer mask blanks.

To summarize the contribution from each of various noise sources, the fluctuation level is plotted as a function of dwell time per pixel for bright field (Figure 2(a)) and for dark field (Figure 2(b)). In Figure 2, instead of plotting 1σ value of the fluctuation, 6σ value of the fluctuation is used because signal to noise ratio of 6σ needs to be obtained to achieve low enough false alarm rate. In deriving these numbers, we assume that the photon flux incident on the bright field detector is 5e8 photons per second, dark field detection efficiency is 7% and that the background scattering corresponds to 0.5% of the bright field signal. The vibration- induced noise is assumed to level off below 10 ms. In Figure 2(a) for the bright field, only vibration and shot noise contributes to the total fluctuation. On the right side of the graph, the signal level expected from defects of 100 nm, 200 nm and 300 nm is denoted. The required dwell time for detecting certain size defect is determined at a point where the 6σ of total noise becomes equal to the signal strength for that defect. In most of the dwell time range, vibration-induced noise dominates over the shot noise level. In fact, the vibration noise is such that ones needs a dwell time of 1 seconds to detect 0.25 % change in the bright field. At the dwell time of 10 msec or below, the signal to noise ratio of 6 or better is achieved only for 500 nm or bigger defects. In the dark field detection, the situation is quite different. The vibration is no longer a dominant noise source while background fluctuation noise dominates at long dwell time and shot noise dominates at short dwell time. Therefore, increasing dwell time beyond 100 msec does not help

to improve the signal to noise ratio due to the spatial-dependent speckle noise. Dwell time of 50 msec is enough to detect 6 % change in the dark field and 10 msec is enough to detect 15 % change in the dark field with good signal to noise ratio. The above analysis shows that the dark field detection holds the most promise to detect 100 nm defects with dwell time as short as 10 msecs. The estimated time for scanning 1 cm^2 of mask blank with 10 msec integration time with 3 μm^2 pixel size[7] is 90 hours[8].

II.2 Number of added defects

The prototype EUV inspection tool resides in an environment where a significant number of particles are added during handling including sample loading/unloading and the pump/vent cycle. The number of added particles during handling is estimated by performing a series of simulated scanning experiments with witness samples. A witness sample, 150 mm Si wafer, is first pre-scanned in the SP1 from KLA-Tencor. The sample is loaded into the chamber, scanned for 2 hours and unloaded. Later the sample is post scanned in the SP1 to obtain the number of added particles. A total of five wafers were used for described experiment. The procedure revealed that the total number of added defects range from 10-20 defects per

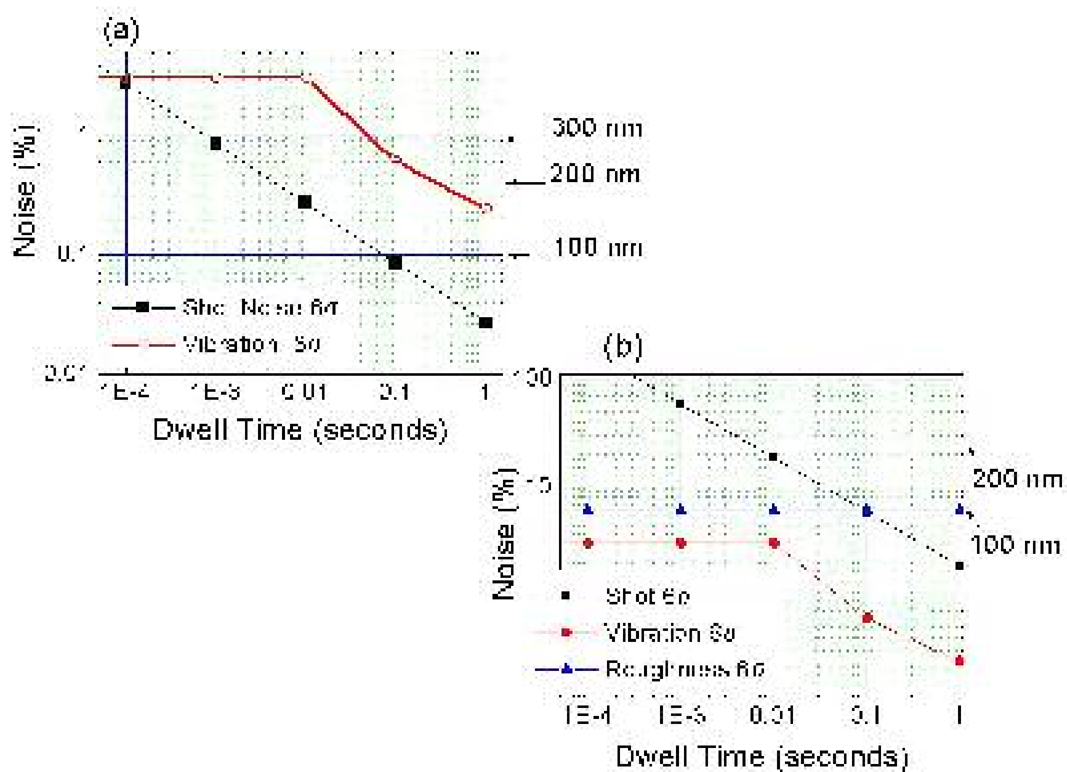

BF	DF	Size 1(nm)	Size 2(nm)
0.12	15	85	94
15	224	1200	1311
0.08	20	80	77
100	--	20000	1311
0.4	41	150	206

cm^2. More than 90 % of these particles have size smaller than 0.3 μm.

III. EXPERIMENTAL PROCEDURE AND RESULTS

As was mentioned in the previous section, the current EUV inspection system adds 10-20 particles per cm^2 when the sample is loaded, scanned and unloaded. These added particles introduce uncertainty in interpreting data when an at-wavelength scanning result is compared with that of the visible inspection tool.

Figure 2. Noise contribution to the bright field fluctuation (a) and to the dark field fluctuation (b) is shown.

In order to identify adders, the sample was pre-scanned in a visible inspection tool so that a defect map before the at-wavelength scan is obtained. After the at-wavelength scan, the sample is scanned in the visible inspection tool again so that the added defects can be discriminated through a map-to-map comparison based on the distance between defects. For this comparison, a large defect can be a useful "registration" reference for small defects.

For the actual experiment, a relatively clean sample was chosen and pre-scanned in the SP1. A region close to the center which did not show any defects was selected for EUV scanning. The total EUV scanning time was 80 hours per cm^2 with pixel size 0.75 μm by 4 μm with dwell time of 10 ms per pixel. A scan was divided into smaller regions of size 10 mm^2 so that the data file size is manageable and the beamline alignment can be re-optimized if beam position drift occurs. After the small region scan, the data is processed to pick up any defect above the threshold as will be explained shortly. If there is a signal above the threshold, a small region (100 by 100 μm typically) in the neighborhood of the above-the-threshold signal region is scanned with time constant of 100 ms in order to determine whether the signal is a false-alarm or a real signal. This procedure repeats until a full 1 cm^2 is covered.

Data processing was performed to compensate or minimize two effects: beam current decay and low frequency vibration. The storage ring current decay is responsible for a gradual decrease in incident photon flux. Therefore, the data value in a row close to the starting position of the scan generally has higher value than the row closer to the end of the scan. In addition, low frequency vibration can introduce a significant variation inside a single row by changing the position of the beam relative to the pinhole. This will introduce a significant signal variation within a single row. This effect needs to be considered when the data is processed. To compensate for these two effects, a numerical high-pass filter has been used for each row of data. After numerical high pass filter, the standard deviation of the row is calculated and the pixels showing signal higher (lower) than 6σ for dark field detection (bright field detection) were tagged as candidates. From 1 cm^2 scanned in this experiment, a total of 100 points showed above-threshold signal. However, when a small area around each defect was rescanned later, only five of them displayed above threshold signal. It is suspected that this high number of false alarms is due to electrical noise. Because the pixel size is smaller than the beam size by a factor of three, a real defect would show above-threshold signal in multiple neighboring pixels. It is indeed the case and when multiple neighboring pixels showed above-threshold signal, the pixel contains a real defect. It can be used as an effective way to decrease the number of false alarms. The bright field and dark field signal strength along with the estimated defect size is listed in Table 1. The bright field signal is in units of % and dark field signal is in units of % relative to the diffuse background scattering. The size was estimated from the chart that was obtained in a cross correlation experiment[2]. From Table 1, there are two defects larger than 1 μm. One of the defects has a size of 20 μm and it was completely opaque. The coordinates of these defects can be used as a registration mark for comparing the coordinates of these defects against those obtained from the visible inspection. When the sample was later scanned in a visible inspection tool (Constellation from ADE) the two large defects were easily identified. From the comparison of distance between defects, the other three defects were also identified. When the distance between defects were compared between coordinates from the EUV inspection tool and the visible inspection tool, the agreement was generally good with +/- 100 μm on average. The size2 shown in Table 1 is the size generated from the visible inspection tool based on the optical scattering cross section. The visible inspection machine classifies defects larger than 1.3 μm as simply 1.3 μm. The agreement between size estimated from EUV inspection and that from the optical inspection tool is reasonable. Furthermore, the smallest defect is classified as 77 nm by optical inspection tool. This demonstrates that the current EUV inspection scheme can detect a very small defect and also that the estimate of 6% dark field increase for 100 nm defect a fairly conservative one. From the comparison between pre-scan and post-scan of the sample, it is concluded that the five defects that the EUV inspection tool detected are added particles during handling and loading. The number five is lower than the average level of adders 10-20 particles per cm^2. Explanation can be sought from the fact that the current sample, when EUV inspection was performed, had not yet experienced a vent/unload cycle while the average added defect density is that of a sample that experienced a full sample loading/pump/vent/unload cycle.

From the current experimental result over 1 cm^2, defects detected by EUV inspection were able to be detected by visible inspection tool. In other words, if there are any defects that are only detectable by EUV inspection, the density is lower than the order of unity per cm^2.

IV. DISCUSSION

In previous sections, the EUV inspection statistics over 1 cm^2 is discussed. A total of five defects were detected from that particular 1 cm^2 and these defects were identified as added particles through comparison between prescan and postscan in the visible inspection tools. Performing EUV inspection over an area large enough to gather defect counting statistics on the order of 0.01 defects per cm^2 would be a very important experiment. The speed of the current EUV inspection tool is limited to 80 hours per cm^2 due to the limited photon flux in the dark field and vibration-induced noise in the bright field as was identified in section II. In this section, an upgrade pathway to improve the scanning speed will be identified.

First, it is worthwhile to review how the total scanning time scales with system configuration and the defect sensitivity. The total scanning time for a given area is computed as the dwell time per pixel(T_0) multiplied by the number of pixels per unit area(N_0). N_0 is determined by dividing the unit area by the pixel size. The pixel size is usually taken to be 1/3 of the beam size. The choice of T_0 and N_0 or the pixel size is constrained by the requirement that the signal to noise ratio needs to be high enough to detect the signal generated by defects of certain size with preset false alarm rate and capture rate. It is rather starighforeard to estimate how the total scan time depends on the spot size and the incident photon flux, when the dominant noise source is photon shot-noise. It is important to keep in mind that in the current scheme, a pinhole is placed in the object plane of the focusing optics and the photons transmitted through the object pinhole are focused onto the sample. When the number of photons per unit area per unit time *incident in the object* pinhole of area A_p is denoted I_0, the photon flux transmitted through the object pinhole is I_0A_p. When these photons pass through the focusing optics of area demagnification M and transmission α, the number of photons reaching the sample is $\alpha I_0 A_p$ and the spot area is A_p/M. After reflection off the sample (EUVL mask blank), the number of photons are further attenuated due to the finite sample reflectivity, detector quantum efficiency and so on. We can lump these loss mechanisms into the optics transmission factor α. Therefore, with dwell time per pixel T_0, the number of photons collected per pixel is $\alpha I_0 A_p T_0$ and the relative fluctuation level (standard deviation divided by the mean) due to the photon shot noise becomes $1/\sqrt{\alpha I_0 A_p T_0}$. The bright field signal from a defect is expected to scale as the ratio of the defect area to the area of the beam, $A_d/(A_p/M)$. Therefore the signal to noise ratio becomes

$$A_d/(A_p/M)\left(\sqrt{\alpha I_0 A_p T_0}\right) = M\frac{A_d}{A_p}\sqrt{\alpha I_0 A_p T_0} .$$

In order to achieve a signal to noise ratio *f* which is determined by the requirement of false alarm and capture rate, the shot noise limited signal to noise ratio should be equal to *f*. In other words,

$$M\frac{A_d}{A_p}\sqrt{\alpha M I_0 T_0} = f .$$

Solving for T_0,

$$T_0 = \frac{A_p}{I_0}\left(\frac{f}{MA_d}\right)^2 .$$

The total number of pixels per unit area is the unit area divided by the pixel size, which is one third of the beam size in the sample plane.

$$N_0 = 3M/A_p .$$

Therefore the total scan time becomes

$$N_0 T_0 = \frac{3}{MI_0}\left(\frac{f}{A_d}\right)^2$$

Form this expression, one can readily notice that the figure of the merit is the product of *incoming photon flux* and *the demagnification of the optical system*. In other words, if we can focus more photons into a

smaller area, the scan time decreases because the increase in the number of pixels (due to smaller spot size) is more than compensated by the decrease in dwell time per pixel (due to the increase in the number of photons per pixel). Therefore, the improvement in scanning rate needs to be sought after in improvement in the photon flux and demagnification ratio. The beamline 11.3.2 (bendmagnet beamline) at the Advanced Light Source at Lawrence Berkeley National Laboratory has photon flux of 5e11 photons per second in a relative bandwidth of 1/730 around 13 nm. The spot size at the beamline focus where the object pinhole is located is 300 μm (horizontal) by 100 μm (vertical) and the full divergence angle is 1.85 mrad in the horizontal and 4.4 mrad in the vertical. The available flux at beamline 11.3.2 can be increased substantially by decreasing the resolving power of the monchromator. In other words, replacing the grating with a plane mirror and a combination of 45 degree angle multilayer mirror enables the collection of photons in the full multilayer bandwidth which is 1/20 FWHM. Therefore, the photon flux within the multilayer bandwidth can be increased by as much as 36 times with this simple approach. Potentially the current EUV inspection system can be improved to scan 1 cm^2 in approximately 2 hours with implementation of this approach, assuming that the vibration due to high scanning speed of the linear stage and optics/sample contamination due to the intense radiation is minimal or mitigated[9]. The beamline or the detector efficiency can be further optimized and further improvement in the scanning speed is possible.

Although increasing the photon flux can improve the scanning speed of the EUV inspection tool, the current prototype tool is limited by the number of added particles and its extendibility into the future defect detection requirements. The issue of added particles can be resolved with the implementation of a commercial robotic sample handling.

Extending the sensitivity of the inspection system is possible with smaller inspection spot size. The sensitivity of the current system is not easily extendible due to the limited spot size improvement. Currently the spot size is limited by aberrations in the glancing angle focusing mirrors. While these types of glancing angle mirrors in Kirkpatrick-Baez configuration have an advantage of low reflectivity loss, being compact, virtually no restriction on the multilayer center wavelength and low cost, it is very hard to achieve a relatively high numerical aperture and low aberrations. Therefore, often the achievable spot size is limited to several microns. A very flexible way to control spot size over a large range is to use normal incidence multilayer coated 20x Schwarzchild optics. (An existing 10x Schwarzchild optics can be modified to a 20x system with a simple change in the distance between two elements[10]). It can deliver diffraction-limited

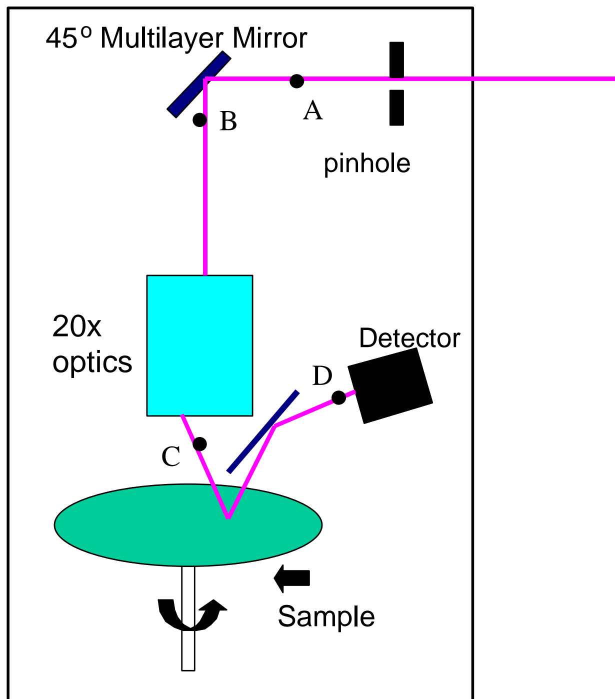

Figure 3. Proposed design of a scanning EUV defect inspection system employing 20x Schwarzchild optics. The beam, after passing through the pinhole, is deflected with a 45 degree multilayer coated mirror and is imaged onto the sample before being captured by the detector assembly.

performance with numerical aperture approaching 0.1. Any spot size down to 0.1 μm FWHM can easily

achieved. Drawbacks for multilayer- coated Schwarzchild optics are its high cost and relatively low photon transmission (~ 30% compared to ~80 % for glancing angle mirror) and its size. In addition, the multilayer coated inspection system requires a mask blank with multilayer period matched to that of the focusing optics.

Figure 3 shows a possible design for the scanning EUV inspection system utilizing 20x Schwarzchild optics. A pinhole of 20 μm is placed in the object plane of the 20x Schwarzchild optics followed by a 45 degree multilayer coated deflection mirror. The pinhole is imaged onto the sample by the 20x Schwarzchild optics. After reflection off the sample, the beam is reflected off another glancing angle mirror before being captured by the detector assembly to alleviate the space constraint imposed by the optics. The sample is mounted on a rotation stage to minimize the vibration induced by the sample movement. The sample is moved with a combination of rotation and radial translation. The photon throughput of the entire optical system from point A to point D can be estimated as 6.5 %(Refer to the endnote for the detailed calculation)[11]. In comparison, the current optical system based on glancing angle mirrors in Kirkpartick-Baez configuration has throughput of 20 % (Refer to the endnote for a detailed calculation)[12]. This factor of three drop in photon throughput in 20 x Schwarzchild focusing system is more than compensated by its higher area demagnification ratio of 400 (20^2) compared to that of the current KB focusing system which is 30[13]. Another optimization is to achieve a tighter focus at the object plane of the pinhole so that the transmitted photon flux is higher. A ray tracing result shows that with an additional horizontal focusing mirror into the beamline, the beamline focus can be tightened as much as four times in the horizontal direction and two times in the vertical direction while the beam divergence remains within the input numerical aperture of the 20x Schwarzchild optics.

When all these improvements are combined, namely (1) full utilization of the synchrotron radiation within the multilayer bandwidth, (2) 20 x multilayer-coated Scwarzchild optics as a focusing element, (3) tighter beamline focus through beamline modification, even a conservative estimate projects that the proposed system can scan 100 cm^2 area of mask blank in approximately 30 hours (approximately 270 times improvement) with the detection sensitivity of 100 nm at beamline 11.3.2 where the current EUV inspection system is installed. In principle, it is possible to further increase the available photon flux and thereby throughput by employing an undulator EUV beamline, BL12.0[14] at the Advanced Light Source at Lawrence Berkeley National Lab, to support the scanning rate of 100 cm^2 in under 10 hours.

ACKNOWLEDGEMENTS

This work is supported by the Extreme Ultraviolet Lithography Limited Liability Company(EUV LLC), the Office of Energy Research, Basic Energy Sciences, of the U.S. Department of Energy under contract No. DE-AC03-76SF00098, SRC contract 96-LC-460 and DARPA grant MDA972-97-1-0010. The authors appreciate help from Dave Richardson for his vibration measurement on mirror tanks in the beamline.

REFERENCES

[1] D. Sweeney, R. Stulen, D. Attwood, and C. Gwyn, "Progress on the development of an EUV lithography system", The 43rd International Conference on Electron, Ion and Photon Beam Technology and Nanofabrication, Marco Island, FL, June 1-4, 1999.

[2] Seongtae Jeong, Chih-Wei Lai, Seno Rekawa, Chris C. Walton, Shon T. Prisbrey, Jeffrey Bokor, " Cross correlation between actinic and visible defect inspection tool for extreme ultraviolet lithography", to be published in Proceedings of SPIE Vol 3873, 19th Annual Symposium on Photomask Technology and Management, Monterey, California, 15-17, September, 1999

[3] S. Jeong, M. Idir, Y. Lin, L. Johnson, S. Rekawa, M. Jones, P. Denham, P. Batson, R. Levesque, P. Kearney, P. Yan, E. Gullikson, J. H. Underwood, J. Bokor, "At-wavelength detection of extreme ultraviolet lithography mask blank defects", Journal of Vacuum Science & Technology B, **16**(6), 3430-3434, Nov-Dec, 1998.

[4] S. Jeong, L. E. Johnson, Y. Lin, S. Rekawa, P. Yan, P.A. Kearney,E. Tejnil, J.H. Underwood, J. Bokor, "Actinic EUVL mask blank defect inspection system", to be published in *Em erging Lithographic Technologies III*, Proceedings of SPIE Vol 3676, Y. Vladimirsky ed., Santa Clara, California, 14-17 March 1999

[5] Because the bright field signal arises from the scattering of photons out of the bright field region into the dark field region as well as the absorption of the EUV radiation, this estimate based on pure absorption is considered to be conservative.
[6] J. H. Underwood, E. M. Gullikson, "Beamline for measurement and characterization of multilayer optics for EUV Lithography", *Emerging Lithographic Technologies II*, Proceedings of SPIE Vol 3331, 52-61, Y. Vladimirsky ed., Santa Clara, California, 23-25 February 1998.
[7] Although, the size of the probe beam is 2.5 by 4 μm with an area of 10 μm^2, there is a reason for the choice of 3 μm^2 (= 0.75 by 4 μm) pixel size. Because the way the data is taken while the stage is in motion, the "effective" spot size becomes the convolution of the pixel size and the actual spot size. When the pixel size is taken 1/3 of the actual spot size, the effective spot size is observed to be indistinguishable from the actual spot size.
[8] Although the spot size is 10 μm^2 (2.5 by 4 μm), the pixel size chosen for the scan is 3 μm^2 (0.75 by 4 μm). Usually, the linear pixel size is 1/3 of the spot size to keep the effective spot size as close to the actual spot size as possible in a continuous scanning scheme. When the pixel size is chosen to be the same as or larger than the beam size, the signal modulation due to a defect is decreased with a loss of signal to noise ratio.
[9] It is well known that the EUV radiation can deposit carbon on an exposed area when the level of hydrocarbon residual gas content is not carefully minimized.
[10] Private conversation with Patrick Naulleau, Lawrence Berkeley National Laboratory.
[11] The 45 degree multilayer mirror, 20x optics, sample and deflection mirror are assumed to have 60%, 30%, 60% and 60% throughput respectively. Therefore from point A to point D, the total throughput would be 0.6x0.3x0.6x0.6 = 6.5 %.
[12] It is assumed that transmission through the KB focusing optics is 80 %, 60% for the sample reflection and 40 % through alignment apertures.
[13] In the current KB focusing system, a 30 by 10 μm pinhole is used to generate 2.5 by 4 μm spot on the sample. Therefore, the area demagnification is 30.
[14] BL 12.0 has been used for interferometric testing of the EUV Lithography optics. See "High-accuracy interferometry of EUV lithographic optical systems," K. A. Goldberg, P. Naulleau, S. Lee, C. Bresloff, D. T. Attwood, and J. Bokor, Proceedings of the EIPBN'98 Conference, Chicago, IL, May 1998, Journal of Vacuum Science and Technology B, 16 (6), 3435-3439 (1998).

Submitted to: **ML01**

Emerging Lithographic Technologies IV Yuli Vladimirsky
(Conference Title) (Conference Chair)

Title: **"Actinic defect counting statistics over 2 cm^2 area of mask blank"**

Authors: Seongtae Jeong[1], Chih-Wei Lai[1,2], Seno Rekawa[1], Chris C Walton[3], Jeffrey Bokor[1,4]

[1] Center for X-Ray Optics, Lawrence Berkeley National Laboratory, Berkeley, CA 94720
[2] Graduate Group of Applied Science and Technology, University of California, Berkeley, CA 94720
[3] Lawrence Livermore National Laboratory, Livermore, CA 94550
[4] Department of Electrical Engineering and Computer Science, University of California, Berkeley, CA 94720

Mailing Address:
Seongtae Jeong: 2-400 Lawrence Berkeley National Laboratory, Berkeley CA 94720
(Phone)(510)486-5048, (Fax)(510)486-4550
(Email) seongtae@grace.lbl.gov
Chih-Wei Lai: 2-400 Lawrence Berkeley National Laboratory, Berkeley CA 94720
(Phone)(510)486-6103, (Fax)(510)486-4550
(Email) eddylai@eecs.berkeley.edu
Seno Rekawa: 2-400 Lawrence Berkeley National Laboratory, Berkeley CA 94720
(Phone)(510)486-6622, (Fax)(510)486-4550
(Email) sbrekawa@lbl.gov
Chris C Walton: L-395 Lawrence Livermore National Laboratory, Livermore CA 94550
(Phone)(925)423-2834 (Fax)
(Email) walton9@llnl.gov
Jeffrey Bokor: Cory Hall, University of California at Berkeley, Berkeley CA94720
(Phone)(510)642-4134 (Fax)(510)642-2739
(Email)jbokor@eecs.berkeley.edu

Oral Presentation

Abstract:

The proposed mask architecture for extreme ultraviolet lithography(EUVL) is a rfefelctive one, consisting of absorber patterns on top of a multilayer reflector. As in other advanced lithographic techniques, the critical defects on mask are one of the major

technical concerns. Especially, the size and density requirements on critical defects on the EUVL mask blank led to active research and development of low-defect density multilayer deposition and inspection technologies.

In previous publications, we have reported on an at-wavelength EUVL mask blank defect inspection system operating at EUV wavelength (11-15 nm) based on scanning mask blank under a focused beam from a synchrotron radiation source at Lawrence Berkeley National Laboratory. Through experiments using programmed defect and cross correlation experiment with visible inspection tools, it has been demonstrated that the current at-wavelength inspection tool can detect sub-100 nm defects. In a recent experiment, we successfully scanned 2 cm^2 area of EUVL mask blank in the current inspection system. In this paper, we will discuss the result of actinic defect counting over the scanned area in comparison with visible inspection results. In addition, a future upgrade path to improve the scanning speed will be discussed.

Keywords: Extreme Ultraviolet Lithography, Mask, defect inspection, at-wavelength

Biography of Seongtae Jeong:

Seongtae Jeong obtained his B.S from Seoul National University, Korea, in 1992 and a Ph.D. from University of California at Berkeley in 1997, both in physics. His graduate research centered on the application of ultrafast laser spectroscopy to carrier dynamics in semiconductors, especially silicon. He joined the Lawrence Berkeley National Laboratory in 1998 as a staff scientist and is currently working on extreme ultraviolet lithography (EUVL) mask blank defect inspection.